

Document downloaded from:

<http://hdl.handle.net/10251/203715>

This paper must be cited as:

Sanchez-Gonzalez, E.; Rodriguez-Rojas, F.; Pinilla-Cienfuegos, E.; Borrero-Lopez, O.; Ortiz, AL.; Guiberteau, F. (2020). Bioinspired design of triboceramics: Learning from the anisotropic microfracture response of dental enamel under sliding contact. *Ceramics International*. 46(18):27983-27989. <https://doi.org/10.1016/j.ceramint.2020.07.292>



The final publication is available at

<https://doi.org/10.1016/j.ceramint.2020.07.292>

Copyright Elsevier

Additional Information

1  
2  
3  
4  
5  
6  
7  
8  
9  
10  
11  
12  
13  
14  
15  
16  
17  
18  
19  
20  
21  
22  
23  
24  
25  
26  
27  
28  
29  
30  
31  
32  
33  
34  
35  
36  
37  
38  
39  
40  
41  
42  
43  
44  
45  
46  
47  
48  
49  
50  
51  
52  
53  
54  
55  
56  
57  
58  
59  
60  
61  
62  
63  
64  
65

**BIOINSPIRED DESIGN OF TRIBOCERAMICS: LEARNING FROM  
THE ANISOTROPIC MICRO-FRACTURE RESPONSE OF DENTAL  
ENAMEL UNDER SLIDING CONTACT**

Estibaliz Sanchez-Gonzalez<sup>a</sup>, Fernando Rodríguez-Rojas<sup>a</sup>,  
Elena Pinilla-Cienfuegos<sup>b</sup>, Oscar Borrero-Lopez<sup>a\*</sup>,  
Angel L. Ortiz<sup>a</sup>, and Fernando Guiberteau<sup>a</sup>

<sup>a</sup> *Departamento de Ingeniería Mecánica, Energética y de los Materiales, Universidad de Extremadura, 06006 Badajoz, Spain*

<sup>b</sup> *Valencia Nanophotonics Technology Center (NTC), Universitat Politècnica de València, Camí de Vera, s/n, 46022 Valencia, Spain*

\*Email: [oborlop@unex.es](mailto:oborlop@unex.es)

1  
2  
3  
4 **Abstract**  
5  
6  
7  
8

9 In the quest for novel ceramics for tribological applications by bioinspired design, the  
10 differences in the fracture modes that arise upon scratching relevant locations of ceramic-  
11 like tooth enamel are investigated. It is found that fracture initiates from weak rod-sheath  
12 interfaces at relatively low loads, independent of the sliding direction. However, the  
13 geometry and propagation of the cracks depends on the orientation of the interfaces  
14 relative to the maximum tensile stress: scratching along the occlusal surface propagates  
15 approximately sinusoidal cracks, parallel to the sliding direction, while scratching along  
16 the cross-section produces straight cracks that propagate normal (scratch parallel to  
17 occlusal surface) or parallel (scratch perpendicular to occlusal surface) to the sliding  
18 direction. Sliding near the enamel-dentine junction hinders the formation of macro-  
19 cracks. Implications for the microstructural design of triboceramics (bulks and coatings)  
20 with improved durability are discussed.  
21  
22  
23  
24  
25  
26  
27  
28  
29  
30  
31  
32  
33  
34  
35  
36  
37  
38  
39  
40  
41  
42  
43  
44

45 *Keywords:* Bioinspired triboceramics; Enamel; Microstructure; Sliding contact; Fracture.  
46  
47  
48  
49  
50  
51  
52  
53  
54  
55  
56  
57  
58  
59  
60  
61  
62  
63  
64  
65

1  
2  
3  
4  
5 **1. Introduction**  
6  
7

8  
9 There is growing interest in developing ceramic materials with microstructures that  
10 imitate those of natural materials such as bone, nacre, spider silk, wood, *etc.*  
11 (biomimetic/bioinspired design) [1, 2]. This is because natural materials have evolved  
12  
13 unique structural features which result in properties that generally excel those of  
14  
15 comparable artificial materials.  
16  
17  
18  
19

20  
21 Among the most remarkable natural materials is dental enamel, the stiffest and  
22  
23 hardest tissue in the human body. Tooth enamel is a ceramic-like protective coating, of  
24  
25 thickness up to ~2.5 mm. It possesses a mostly mineral (> 95 wt%), complex hierarchical  
26  
27 microstructure. The basic structural units are elongated hydroxyapatite crystals, separated  
28  
29 by a thin protein layer (nanostructure). The crystals bundle together into tightly packed  
30  
31 rods of approximately 5  $\mu\text{m}$  diameter and high aspect ratio, separated by less mineralized  
32  
33 sheaths. In turn, rods align parallel to the surface in the outer enamel and intertwine in the  
34  
35 inner enamel, which is known as decussation, forming patterns that vary between species.  
36  
37  
38 As a result of its unique microstructure, the enamel shows a damage tolerance that goes  
39  
40 beyond otherwise modest values of fracture strength and toughness [3, 4].  
41  
42  
43  
44

45  
46 Based on the above, microstructural design inspired by tooth enamel has the  
47  
48 potential to improve the properties of ceramic materials that perform comparable  
49  
50 functions. In order to optimize the design of such bioinspired triboceramics, it is first  
51  
52 critical to know how the highly anisotropic microstructure of enamel responds under  
53  
54 different loading conditions. In this context, previous studies have focused on the  
55  
56 variation within the enamel surface and cross-section of mechanical properties such as  
57  
58 elastic modulus, hardness, fracture strength and toughness, at different length-scales, by  
59  
60  
61  
62  
63  
64  
65

1  
2  
3  
4 means of micro/nanoindentation [5-7], compact-tension [6, 8], and tensile tests [9],  
5  
6 among others.

7  
8  
9 One aspect of prime importance to enamel is wear resistance. Indeed, despite its  
10 remarkable properties, the enamel is vulnerable in the long-term to cumulative damage  
11 from repetitive contacts, especially those involving high lateral forces during mastication  
12 and bruxism/tooth grinding [10, 11]. If severe, enamel wear can compromise its  
13 functionality and ultimately limit its durability [12]. Accordingly, the macroscopic  
14 tribological response of enamel has been extensively investigated by various wear tests  
15 [12-16], conducted mostly on occlusal surfaces. To complement those, scratch tests have  
16 been used, albeit to a lesser extent, in order to probe the fundamental damage  
17 mechanisms generated by individual sliding micro-contacts at the particle/asperity level  
18 [17-20]. However, those previous scratch studies typically employed very small tips,  
19 which can only probe the response of individual rods, or regions within individual rods  
20 (*i.e.*, the nanoscale). Moreover, very small tips generate damage mostly by plastic  
21 deformation, and thus simulate damage mechanisms pertaining to the mild-wear regime  
22 [21]. Therefore, the fundamental fracture response of the enamel under sliding contacts at  
23 the microstructural scale (*i.e.*, spanning a few rods) remained to be investigated. This  
24 aspect is critical because such response in turn determines material removal processes in  
25 the severe-wear region [21].

26  
27  
28 To address this issue, the present work examines the scratch damage along  
29 relevant parts of the enamel microstructure, namely the occlusal surface, the outer enamel  
30 cross-section (sliding both parallel and perpendicular to the rods' axis), and the inner  
31 enamel cross-section. Special attention is paid to the formation of cracks in each case.

1  
2  
3  
4 The conclusions drawn from this work are expected to provide valuable insight for the  
5  
6 development of both bulk triboceramics and anti-wear ceramic coatings inspired by tooth  
7  
8 enamel with improved resistance to damage from sliding contacts, and ultimately with  
9  
10 improved durability.  
11  
12  
13  
14

## 15 16 **2. Materials and methods** 17 18 19 20

21 Dental samples were provided by local dentists. In particular, impacted or semi-impacted  
22  
23 wisdom teeth free of damage and of healthy appearance were collected from young adult  
24  
25 patients. Enamel specimens were prepared from the supplied molars. First, individual  
26  
27 teeth were embedded in the axial direction in a cylindrical pellet of cold-curing resin.  
28  
29 Occlusal surfaces for testing were then obtained by lightly grinding the top of the pellet  
30  
31 until there were flat surfaces of width  $\sim 1.5$  mm at the molar cusps, and cross-sectional  
32  
33 surfaces were obtained by cutting perpendicular to the occlusal surface. Test surfaces  
34  
35 were subsequently polished to a  $1 \mu\text{m}$  finish using a conventional ceramographic routine.  
36  
37 Finally, the surface opposite the polished test surface was flattened in order to ensure that  
38  
39 the resulting specimens were perfectly plane parallel. Throughout the entire sample  
40  
41 preparation process, specimens were kept hydrated as much as possible. Preliminary  
42  
43 Vickers microindentation tests at a 200 g load were conducted on the polished occlusal  
44  
45 surfaces, and only samples from teeth of measured hardness values between 3.5 GPa and  
46  
47 4.5 GPa, typical of sound enamel, were finally selected for subsequent scratch testing in  
48  
49 order to ensure that the samples were comparable [22].  
50  
51  
52  
53  
54  
55  
56  
57  
58  
59  
60  
61  
62  
63  
64  
65

1  
2  
3  
4 Scratch tests were performed in a dedicated device (Revetest RST3, Anton Paar,  
5  
6 Graz, Austria) using a Rockwell-C diamond tip of radius 200  $\mu\text{m}$ , at ambient conditions  
7  
8 without lubrication. Tests at both constant load (CL) and progressive load (PL) were  
9  
10 conducted. In the CL tests, a normal load of 5 N was employed. From the scratch widths  
11  
12 measured after the CL tests, scratch hardness values were calculated according to [23]. In  
13  
14 the PL tests, the normal load was increased from 1 N to 10 N. In both the CL and PL  
15  
16 tests, the sliding speed was 0.5 mm/min and the scratch length was 0.5 mm. Tests were  
17  
18 performed on polished occlusal and cross-sectional surfaces. On the cross-section, tests  
19  
20 were performed on the outer enamel, sliding both parallel and perpendicular to the  
21  
22 occlusal surface (*i.e.*, sliding perpendicular and parallel to the direction of alignment of  
23  
24 the rods, respectively). Finally, tests on the cross-section's inner enamel were also  
25  
26 performed, sliding parallel to the enamel-dentine junction (EDJ). The location of the  
27  
28 scratch tests in the different parts of the enamel is indicated schematically in Fig. 1,  
29  
30 together with micrographs representative of the microstructure at each location.  
31  
32  
33  
34  
35  
36  
37

38 The surface of the specimens after testing was inspected by optical microscopy  
39  
40 (OM, Epiphot 300, Nikon, Tokyo, Japan) and scanning electron microscopy (SEM, S-  
41  
42 3600N, Hitachi, Japan). The SEM images were collected with secondary electrons in  
43  
44 relatively low vacuum to minimize specimen dehydration.  
45  
46  
47

48 High resolution Raman spectral imaging (Raman/AFM alpha300 RA, Witec,  
49  
50 Germany) was performed in selected cases, using lens magnification  $\times 50$ , laser  
51  
52 wavelength 532 nm, grating 600 l/mm, spectral resolution 2-3  $\text{cm}^{-1}$  per CCD pixel, lateral  
53  
54 resolution  $\approx 500$  nm, axial resolution (confocal)  $\approx 3\mu\text{m}$ . Specifically, Raman spectra were  
55  
56 collected at every measurement point (Fig. 1(B):  $150 \times 150$  points, 0.5 s integration time,  
57  
58  
59  
60  
61  
62  
63  
64  
65

1  
2  
3  
4 Fig. 1(C): 180 × 180 points, 0.03615 s integration time, Fig. 5(C): 180 × 120 points, 0.05  
5  
6 s integration time), so that, in a single Raman image (Fig. 1(B): 40 μm × 40 μm scan,  
7  
8 Fig. 1(C): 90 μm × 90 μm scan, Fig. 5(C): 60 μm × 40 μm scan), multiple mineral  
9  
10 species (each represented by its own Raman spectrum) could be acquired.  
11  
12

13  
14 Despite being time consuming, Raman spectroscopy has the advantage that it can  
15  
16 clearly reveal the microstructure of the enamel, which otherwise is difficult to image with  
17  
18 other techniques such as OM and SEM, by analyzing the characteristic peaks of  
19  
20 hydroxyapatite ( $\text{Ca}_{10}(\text{PO}_4)_6(\text{OH})_2$ ), the main mineral component of enamel. In particular,  
21  
22 the Raman images were generated from changes of  $963 \text{ cm}^{-1}$  phosphate ( $\text{PO}_4$ ) Raman  
23  
24 peak that correspond to the  $\nu_1$  symmetric stretching mode of  $\text{PO}_4$ , and is the sharpest and  
25  
26 most intense band of the enamel [22].  
27  
28  
29  
30  
31  
32

### 33 34 **3. Results**

35  
36  
37  
38  
39 The scratch hardness values calculated from the measured widths of the scars in the CL  
40  
41 tests at different locations are shown in Fig. 2. The highest average value is obtained  
42  
43 when sliding is performed along the occlusal surface. The average value is only slightly  
44  
45 lower when sliding is performed along the cross-section in the outer enamel, but  
46  
47 significantly lower in the inner enamel near the EDJ in order to minimize the mismatch  
48  
49 with the softer dentine. The scratch hardness values are consistent with measurements  
50  
51 performed by instrumented indentation in different locations of the enamel [5].  
52  
53

54  
55  
56 The values of the coefficient of friction (CoF) obtained in the PL scratch tests are  
57  
58 shown in Fig. 3. The CoF increases with increasing normal load as a result of an  
59  
60  
61  
62  
63  
64  
65



1  
2  
3  
4 expanding contact zone, from a value of  $\sim 0.05$  at the beginning of the test up to  $\sim 0.12$  at  
5  
6  
7 the end. These are relatively low values [24], which attest to the ease of sliding of enamel  
8  
9 as required for efficient mastication using a combination of normal and lateral forces.  
10  
11 There are no significant differences in the CoF values obtained along the different  
12  
13 directions of the enamel. However, sliding near the EDJ produced more fluctuating  
14  
15 curves, which is attributable to a somewhat rougher surface resulting from the more  
16  
17 intense decussation of the enamel rods in that region [3, 4].  
18  
19

20  
21 Low-magnification optical images of the scratch tracks produced by the PL tests  
22  
23 are shown in Fig. 4. As expected, the widths of the tracks increase as the applied load is  
24  
25 increased. In all cases, the initial damage at low loads occurs by ‘plastic’ (*i.e.*, permanent)  
26  
27 deformation. This is followed by fracture at intermediate loads, with cracks initiated  
28  
29 preferentially near the edges of the contact zone. Critically, the crack geometry shows a  
30  
31 marked dependence on the location of the scratch test in the enamel. In particular, sliding  
32  
33 along the occlusal surface produces cracks of approximately sinusoidal contours, with  
34  
35 amplitudes of a few micrometres, that extend parallel to the sliding direction (circled  
36  
37 areas in Fig. 4(A)). In contrast, sliding along the outer enamel cross-section produces  
38  
39 more straight cracks that are either preferentially perpendicular (circled area in Fig. 4(B))  
40  
41 or parallel (Fig. 4(C)) to the sliding direction, when sliding parallel and perpendicular to  
42  
43 the occlusal surface, respectively. Within the data scatter, no significant differences were  
44  
45 observed in the loads at which the first cracks appear — in all cases, the normal loads at  
46  
47 first cracking were between  $\approx 3$ -5 N. Finally, larger cracks appear to be suppressed upon  
48  
49 sliding along the inner cross-section, near the EDJ (Fig. 4(D)).  
50  
51  
52  
53  
54  
55  
56  
57  
58  
59  
60  
61  
62  
63  
64  
65

#### 4. Discussion

In order to explain the observed differences in crack geometry as a function of the test location, two aspects need to be taken into account: ‘flaws’, that is, weaker microstructural elements from which cracks will initiate, and the stress field that drives the propagation of cracks. In biphasic ceramics, the interfaces between phases of different properties are typically regarded as the weakest link of the microstructure [25, 26]. In the particular case of enamel, the sheaths have less mineralized content than the bulk of the rods. As a result, rod-sheath interfaces are potential precursors of failure there. In regards to the applied stress, in a sliding contact the highest tensile component is localized at the trailing edge of the contact, and has a radial orientation on the surface [27]. Because the stress ahead of the tip is compressive, in isotropic ceramics this field thus opens flaws oriented normal to the tensile stress (mode I), producing cracks along the contours of the moving contact edge, but only in the trailing half — the so-called partial ring/cone cracks [28]. In ceramics with an anisotropic microstructure like enamel, the crack pattern differs from partial ring cracks because the precursor flaws and paths of least resistance are not homogeneously distributed relative to the tensile stress [29-32].

Note that in the present scratch tests the magnitude of the tensile stress for a given applied load is expected to be largely independent of the location in the enamel and sliding direction considered — except for the softer region of the inner enamel near the EDJ — as the measured values of CoF are very similar in all cases (Fig. 3) [27]. Consequently, the differences in the geometry of the cracks as a function of location in

1  
2  
3  
4 the enamel are attributable to the specific geometry and orientation of the weak rod-  
5  
6 sheath interfaces in each case.  
7

8  
9 In the occlusal surface, all sliding directions are equivalent because the rods are  
10 oriented with their longer axis normal to the surface. This orientation exposes their  
11 approximately circular cross-sections (Fig. 1(B)). As a result, micro-cracks pop-in from  
12 flaws at the circular interfaces, as illustrated schematically in Fig. 5(A). As the tip moves  
13 along, similar micro-cracks subsequently nucleate. Connection between adjacent micro-  
14 cracks thus results in cracks of approximately sinusoidal contours, extending parallel to  
15 the sliding direction but skirting the rods, with amplitudes comparable to the rod diameter  
16 (~5 $\mu$ m) (Figs. 5(B) and 5(C)). This particular crack geometry is also commonly observed  
17 in the radial cracks emanating from sharp indentations on occlusal surfaces [6].  
18  
19  
20  
21  
22  
23  
24  
25  
26  
27  
28  
29  
30

31 In the cross-section of the outer enamel, rods are aligned with their longer axis  
32 parallel to the exposed contact surface (Fig. 1(C)), with an increasing degree of  
33 intertwining as the distance from the occlusal surface increases [3, 4]. Thus, unlike the  
34 case at the occlusal surface, the scratch direction determines the relative orientation of the  
35 weak interfaces. In particular, when scratching parallel to the occlusal surface (*i.e.*,  
36 perpendicular to the rods' axis), the flaws developed at the interface are predominantly  
37 oriented perpendicular to the sliding direction (Fig. 6(A)), which results in straight cracks  
38 propagating along sheaths normal to it (Figs. 6(B) and 6(C)). On the contrary, scratching  
39 perpendicular to the occlusal surface (*i.e.*, parallel to the rods' axis) results predominantly  
40 (but not exclusively) in cracks propagating along sheaths parallel to the sliding direction  
41 (Figs. 7(A)-(C))<sup>1</sup>.  
42  
43  
44  
45  
46  
47  
48  
49  
50  
51  
52  
53  
54  
55  
56  
57  
58

---

59 <sup>1</sup> Note that rod decussation in actual enamel samples to some extent distorts the idealized crack geometries  
60 depicted in Figs. 6(A) and 7(A).  
61  
62  
63  
64  
65

1  
2  
3  
4 It is important to note that, despite the observed differences in crack geometry, the  
5  
6 critical load at which fracture initiates does not show a significant dependence on the  
7  
8 location of the scratch test in the enamel, suggesting a similar population of exposed  
9  
10 flaws in all cases. The exception is the region near the EDJ, where the lower mineral  
11  
12 content and higher extent of decussation [3, 4] result in lower hardness (Fig. 2), with the  
13  
14 concordant suppression of larger cracks. Moreover, the relatively low contact loads at  
15  
16 which the first cracks are observed in the PL tests ( $F_N=3-5$  N) reveal the weakness of the  
17  
18 rod-sheath interfaces and suggest a low short-crack toughness. This is in good agreement  
19  
20 with the experimental values reported elsewhere [8] in the range  $0.5-0.8$  MPa·m<sup>1/2</sup> in  
21  
22 occlusal surfaces and cross-sections.  
23  
24  
25  
26  
27

28  
29 In isotropic ceramics, interfacial weakness/low short-crack toughness are  
30  
31 associated with poor wear resistance in the severe-wear regime [25]. However, it is  
32  
33 important to note that, in the enamel, this limitation can be overcome by the anisotropic  
34  
35 nature of its microstructure. A key aspect is the location of the weak interfaces. Indeed,  
36  
37 removal processes in the severe-wear regime are largely governed by the propagation of  
38  
39 surface (radial) and especially sub-surface (lateral) cracks [21]. The latter are expected to  
40  
41 be facilitated when the weak interfaces are aligned parallel to the surface.  
42  
43  
44

45  
46 Based on the above, and considering the results of this study, it is hypothesized  
47  
48 that the cracks induced by sliding contacts at the occlusal surface (Fig. 5) are relatively  
49  
50 safe and less likely to lead to material loss than others. This is because, even if such  
51  
52 cracks completely circumvent individual (or bundles of) rods, their orientation with the  
53  
54 longer axis normal to the surface (*i.e.*, weak interfaces normal to the surface) makes it  
55  
56 difficult to remove them [33]. This is consistent with previous studies that indicate that  
57  
58  
59  
60  
61  
62  
63  
64  
65

1  
2  
3  
4 the occlusal surface of enamel has a higher wear resistance than artificial biphasic dental  
5  
6 ceramics with better mechanical properties but isotropic microstructures [13].  
7  
8

9         Comparatively, cracks generated in a contact surface with the microstructural  
10 arrangement of the enamel cross-section are more likely to result in wear. This is because  
11 the orientation of rods in this case, with their shortest dimension normal to the surface  
12 (*i.e.*, weak interfaces parallel and close to the surface), makes them vulnerable to  
13 wholesale pull-out when cracks circumvent them and coalesce [33]. These assertions are  
14 in agreement with the experimental results obtained by others who report greater  
15 macroscopic wear in tests conducted at the enamel cross-section than at the occlusal  
16 surface [16].  
17  
18  
19  
20  
21  
22  
23  
24  
25  
26  
27

28         This work has relevant implications for the design of bioinspired ceramics based  
29 on the structure of natural enamel for tribological applications. These not only include  
30 bulk ceramics for dental prostheses, processed for example by 3-D printing techniques [1,  
31 4, 34, 35], but also anti-wear ceramic coatings obtained from a vapour phase to use in  
32 milling, grinding and cutting tools, which commonly have columnar, enamel-like  
33 microstructures [36]. Such structures are based on different arrangements of high aspect  
34 ratio crystals (or polycrystalline rods) bonded by a matrix. The results obtained here  
35 reveal that, while this type of microstructure has a relatively low resistance to cracking  
36 from sliding contacts, which initiates at weak interfaces, an appropriate arrangement can  
37 result in materials in which the interfacial weakness is not necessarily deleterious to the  
38 wear resistance. In particular, it can be argued that the arrangement present at the occlusal  
39 surface of natural enamel (crystals/rods oriented with their longest axis normal to surface)  
40 hinders crystal/rod pull-out because there are no weak interfaces parallel and close to the  
41  
42  
43  
44  
45  
46  
47  
48  
49  
50  
51  
52  
53  
54  
55  
56  
57  
58  
59  
60  
61  
62  
63  
64  
65

1  
2  
3  
4 surface, and this results in materials with a potentially higher wear resistance than the  
5  
6 other possible configurations. This type of bioinspired microstructural arrangement is  
7  
8 thus capable of overcoming one of the classic limitations of conventional biphasic  
9  
10 ceramics [25, 26]. Applied to the enamel-like structures commonly seen in coatings/thin  
11  
12 films, the present observations suggest that a columnar microstructure (*e.g.*, CVD  
13  
14 coatings [36]) is likely to attain greater wear resistance than a lamellar one (*e.g.*, plasma-  
15  
16 sprayed coatings[37]), and that one possible strategy to further improve the resistance in  
17  
18 the former is by developing Zone T microstructures with intertwined columns [36].  
19  
20  
21  
22  
23  
24

## 25 26 **5. Conclusions**

27  
28  
29  
30  
31 To extract guidelines for the microstructural design of bioinspired triboceramics with  
32  
33 improved durability, we have investigated the differences in the fracture modes that arise  
34  
35 upon scratching relevant locations of ceramic-like tooth enamel: occlusal surface, and  
36  
37 cross-section sliding both parallel and perpendicular to the axis of the rods. Based on the  
38  
39 results and analyses, the following conclusions can be drawn:  
40  
41  
42  
43  
44

- 45  
46 1. Fracture initiates from weak rod-sheath interfaces at relatively low loads,  
47  
48 independent of the location in the enamel and direction of sliding.  
49
- 50  
51 2. The geometry of the cracks depends on the orientation of the weak interfaces  
52  
53 relative to the maximum tensile stress: scratching along the occlusal surface  
54  
55 produces approximately sinusoidal cracks along sheaths, parallel to the sliding  
56  
57 direction, while scratching along the cross-section in the outer enamel produces  
58  
59  
60  
61  
62  
63  
64  
65

1  
2  
3  
4 straight cracks, normal (scratch parallel to the occlusal surface) or parallel  
5  
6  
7 (scratch perpendicular to the occlusal surface) to the sliding direction. Sliding  
8  
9 near the enamel-dentine junction hinders the formation of larger cracks.

- 10  
11  
12 3. Orientation of rods (and thus of weak interfaces) perpendicular to the contact  
13  
14 surface makes them less vulnerable to pull-out compared to orientation parallel to  
15  
16 the surface.  
17  
18  
19 4. Bioinspired triboceramics with improved durability should be designed by  
20  
21 carefully orienting the longest dimension of reinforcement phases perpendicular  
22  
23 to the contact surface, as in occlusal enamel.  
24  
25  
26  
27

## 28 **Acknowledgements**

29  
30  
31  
32

33 The authors wish to thank Dr Florencio Monje Gil for kindly providing tooth specimens  
34 from his clinic (CICOM, Centro de Implantología Cirugía Oral y Maxilofacial, Badajoz,  
35 Spain). This study was supported by Junta de Extremadura, Spain, and FEDER/ERDF  
36 funds (grants IB16139 and GR18149). E. P.-C. gratefully acknowledges support from the  
37 Spanish Ministry of Economy and Competitiveness (MINECO) under grant FJCI-2015-  
38  
39  
40  
41  
42  
43  
44  
45  
46 27228.  
47  
48  
49  
50  
51  
52  
53  
54  
55  
56  
57  
58  
59  
60  
61  
62  
63  
64  
65

1  
2  
3  
4 **Figure captions**  
5  
6  
7  
8

- 9  
10  
11  
12  
13  
14  
15  
16  
17  
18  
19  
20  
21  
22  
23  
24  
25  
26  
27  
28  
29  
30  
31  
32  
33  
34  
35  
36  
37  
38  
39  
40  
41  
42  
43  
44  
45  
46  
47  
48  
49  
50  
51  
52  
53  
54  
55  
56  
57  
58  
59  
60  
61  
62  
63  
64  
65
1. (A) Montage of several optical micrographs collected on polished surfaces, indicating the different locations on the enamel where scratch tests were conducted: occlusal (direction (1)); cross-section, parallel to the occlusal surface (direction (2)); cross-section, perpendicular to the occlusal surface (direction (3)); cross-section, parallel to the enamel-dentine junction, EDJ (direction (4)). Microstructure of the enamel observed by Raman spectroscopy: (B) at the occlusal surface (Raman image: Scan 40  $\mu\text{m}$  x 40  $\mu\text{m}$ , 963  $\text{cm}^{-1}$  peak), and (C) at the cross-section, below the occlusal surface (Raman image: Scan 90  $\mu\text{m}$  x 90  $\mu\text{m}$ , 963  $\text{cm}^{-1}$  peak).
  2. Plot of scratch hardness measured from tests at constant load, as a function of location in the enamel and sliding direction.
  3. Plot of coefficient of friction *vs* sliding distance obtained from scratch tests at progressive load along the locations indicated in Fig. 1.
  4. Panoramic optical micrographs of the tracks obtained after scratch tests at progressive loading at different locations of the enamel: (A) occlusal surface; (B) cross-section, sliding parallel to occlusal surface; (C) cross-section, sliding normal to occlusal surface; (D) cross-section, near the enamel-dentine junction, corresponding respectively to directions (1), (2), (3), and (4) in Fig. 1(A). The broken white lines mark characteristic fracture modes (higher magnification



1  
2  
3  
4 details are provided in Figs. 5-7).  
5  
6  
7

- 8  
9 5. Scratch fracture on the enamel occlusal surface (corresponding to direction (1) in  
10 Fig. 1(A)): (A) schematic diagram indicating the orientation of precursor flaws (in  
11 red) relative to the maximum tensile stress field (in black), superimposed on the  
12 microstructure (not to scale), with blue arrow indicating the sliding direction; (B)  
13 optical micrograph showing a detail of a characteristic, approximately sinusoidal,  
14 crack; (C) higher magnification detail obtained by Raman spectroscopy (Raman  
15 image: Scan 60  $\mu\text{m}$  x 40  $\mu\text{m}$ , 963  $\text{cm}^{-1}$  peak).  
16  
17  
18  
19  
20  
21  
22  
23  
24  
25  
26  
27  
28 6. Scratch fracture on the enamel cross-section, sliding parallel to the occlusal  
29 surface (corresponding to direction (2) in Fig. 1(A)): (A) schematic diagram  
30 indicating the orientation of precursor flaws (in red) relative to the maximum  
31 tensile stress field (in black), superimposed on the microstructure (not to scale),  
32 with blue arrow indicating the sliding direction; (B) optical micrograph showing a  
33 detail of the characteristic cracks normal to the sliding direction; (C) higher  
34 magnification detail obtained by SEM.  
35  
36  
37  
38  
39  
40  
41  
42  
43  
44  
45  
46  
47 7. Scratch fracture on the enamel cross-section, sliding perpendicular to the occlusal  
48 surface (corresponding to direction (3) in Fig. 1(A)): (A) schematic diagram  
49 indicating the orientation of precursor flaws (in red) relative to the maximum  
50 tensile stress field (in black), superimposed on the microstructure (not to scale),  
51 with blue arrow indicating the sliding direction; (B) optical micrograph showing a  
52 detail of the characteristic cracks parallel to the sliding direction, pointed by white  
53  
54  
55  
56  
57  
58  
59  
60  
61  
62  
63  
64  
65

arrows; (C) higher magnification detail obtained by SEM.

## References

- [1] U.G.K. Wegst, H. Bai, E. Saiz, A.P. Tomsia, R.O. Ritchie, Bioinspired structural materials, *Nature Materials* 14(1) (2015) 23-36.
- [2] H.J. Gao, B.H. Ji, I.L. Jager, E. Arzt, P. Fratzl, Materials become insensitive to flaws at nanoscale: Lessons from nature, *Proceedings of the National Academy of Sciences of the United States of America* 100(10) (2003) 5597-5600.
- [3] J. Wilmers, S. Bargmann, Nature's design solutions in dental enamel: Uniting high strength and extreme damage resistance, *Acta Biomaterialia* 107 (2020) 1-24.
- [4] V.P. Thompson, The tooth: An analogue for biomimetic materials design and processing, *Dental Materials* 36(1) (2020) 25-42.
- [5] J.L. Cuy, A.B. Mann, K.J. Livi, M.F. Teaford, T.P. Weihs, Nanoindentation mapping of the mechanical properties of human molar tooth enamel, *Archives of Oral Biology* 47(4) (2002) 281-291.
- [6] D. Bajaj, S. Park, G.D. Quinn, D. Arola, Fracture Processes and Mechanisms of Crack Growth Resistance in Human Enamel, *Jom* 62(7) (2010) 76-82.
- [7] B.B. An, R.R. Wang, D. Arola, D.S. Zhang, The role of property gradients on the mechanical behavior of human enamel, *Journal of the Mechanical Behavior of Biomedical Materials* 9 (2012) 63-72.
- [8] M. Yahyazadehfar, D. Bajaj, D.D. Arola, Hidden contributions of the enamel rods on the fracture resistance of human teeth, *Acta Biomaterialia* 9(1) (2013) 4806-4814.
- [9] M. Giannini, C.J. Soares, R.M. de Carvalho, Ultimate tensile strength of tooth structures, *Dental Materials* 20(4) (2004) 322-329.
- [10] P.S. Ungar, *Teeth: A Very Short Introduction*, Oxford University Press, Oxford, UK, 2014.
- [11] T.M. Smith, *The tales teeth tell*, The MIT Press, Cambridge, MA, 2018.
- [12] O. Borrero-Lopez, A. Pajares, P.J. Constantino, B.R. Lawn, A model for predicting wear rates in tooth enamel, *Journal of the Mechanical Behavior of Biomedical Materials* 37 (2014) 226-234.
- [13] O. Borrero-Lopez, F. Guiberteau, Y. Zhang, B.R. Lawn, Wear of ceramic-based dental materials, *Journal of the Mechanical Behavior of Biomedical Materials* 92 (2019) 144-151.
- [14] F. Santos, A. Branco, M. Polido, A.P. Serro, C.G. Figueiredo-Pina, Comparative study of the wear of the pair human teeth/Vita Enamic (R) vs commonly used dental ceramics through chewing simulation, *Journal of the Mechanical Behavior of Biomedical Materials* 88 (2018) 251-260.
- [15] J.A. Arsecularatne, M. Hoffman, Ceramic-like wear behaviour of human dental enamel, *Journal of the Mechanical Behavior of Biomedical Materials* 8 (2012) 47-57.
- [16] J. Zheng, Z.R. Zhou, J. Zhang, H. Li, H.Y. Yu, On the friction and wear behaviour of human tooth enamel and dentin, *Wear* 255 (2003) 967-974.

- 1  
2  
3  
4 [17] Y.F. Jia, F.Z. Xuan, Anisotropic wear behavior of human enamel at the rod level in  
5 terms of nanoscratching, *Wear* 290 (2012) 124-132.
- 6 [18] G. Guidoni, M. Swain, I. Jager, Nano-scale sliding contact deformation behaviour of  
7 enamel under wet and dry conditions, *Journal of Materials Science-Materials in Medicine*  
8 21(4) (2010) 1195-1203.
- 9 [19] P.W. Lucas, M. Wagner, K. Al-Fadhalah, A.S. Almusallam, S. Michael, L.A. Thai,  
10 D.S. Strait, M.V. Swain, A. van Casteren, W.M. Renno, A. Shekeban, S.M. Philip, S.  
11 Saji, A.G. Atkins, Dental abrasion as a cutting process, *Interface Focus* 6(3) (2016).
- 12 [20] J. Xia, Z.R. Tian, L.C. Hua, L. Chen, Z.R. Zhou, L.M. Qian, P.S. Ungar, Enamel  
13 crystallite strength and wear: nanoscale responses of teeth to chewing loads, *Journal of*  
14 *the Royal Society Interface* 14(135) (2017).
- 15 [21] O. Borrero-Lopez, A. Pajares, P.J. Constantino, B.R. Lawn, Mechanics of  
16 microwear traces in tooth enamel, *Acta Biomaterialia* 14 (2015) 146-153.
- 17 [22] E. Sanchez-Gonzalez, E. Pinilla-Cienfuegos, O. Borrero-Lopez, F. Rodriguez-Rojas,  
18 F. Guiberteau, Contact damage of human dental enamel under cyclic axial loading with  
19 abrasive particles, *Journal of the Mechanical Behavior of Biomedical Materials* 102  
20 (2020).
- 21 [23] A. International, ASTM G171 - 03(2017), Standard Test Method for Scratch  
22 Hardness of Materials Using a Diamond Stylus, ASTM International, West  
23 Conshohocken, PA, 2017,.
- 24 [24] K. Kato, Tribology of ceramics, *Wear* 136(1) (1990) 117-133.
- 25 [25] B.R. Lawn, Fracture of brittle solids, Cambridge University Press, Cambridge,UK,  
26 1993.
- 27 [26] B.R. Lawn, N.P. Padture, H.D. Cai, F. Guiberteau, Making ceramics ductile, *Science*  
28 263(5150) (1994) 1114-1116.
- 29 [27] G.M. Hamilton, L.E. Goodman, Stress field created by a circular sliding contact,  
30 *Journal of Applied Mechanics* 33(2) (1966) 371-&.
- 31 [28] B.R. Lawn, Partial cone crack formation in a brittle material loaded with a sliding  
32 spherical indenter, *Proceedings of the Royal Society of London Series a-Mathematical*  
33 *and Physical Sciences* 299(1458) (1967) 307-&.
- 34 [29] O. Borrero-Lopez, T. Vodenitcharova, M. Hoffman, Anisotropy effects on the  
35 reliability of single-crystal silicon, *Scripta Materialia* 63(10) (2010) 997-1000.
- 36 [30] T. Vodenitcharova, O. Borrero-Lopez, M. Hoffman, Mechanics prediction of the  
37 fracture pattern on scratching wafers of single crystal silicon, *Acta Materialia* 60(11)  
38 (2012) 4448-4460.
- 39 [31] H.J. Leu, R.O. Scattergood, Sliding contact fracture on glass and silicon, *Journal of*  
40 *Materials Science* 23(8) (1988) 3006-3014.
- 41 [32] O. Borrero-Lopez, M. Hoffman, A. Bendavid, P.J. Martin, Mechanical properties  
42 and scratch resistance of filtered-arc-deposited titanium oxide thin films on glass, *Thin*  
43 *Solid Films* 519(22) (2011) 7925-7931.
- 44 [33] M.C. Maas, E.R. Dumont, Built to last: The structure, function, and evolution of  
45 primate dental enamel, *Evolutionary Anthropology* 8(4) (1999) 133-152.
- 46 [34] E. Feilden, C. Ferraro, Q.H. Zhang, E. Garcia-Tunon, E. D'Elia, F. Giuliani, L.  
47 Vandeperre, E. Saiz, 3D Printing Bioinspired Ceramic Composites, *Scientific Reports* 7  
48 (2017).
- 49  
50  
51  
52  
53  
54  
55  
56  
57  
58  
59  
60  
61  
62  
63  
64  
65

1  
2  
3  
4  
5  
6  
7  
8  
9  
10  
11  
12  
13  
14  
15  
16  
17  
18  
19  
20  
21  
22  
23  
24  
25  
26  
27  
28  
29  
30  
31  
32  
33  
34  
35  
36  
37  
38  
39  
40  
41  
42  
43  
44  
45  
46  
47  
48  
49  
50  
51  
52  
53  
54  
55  
56  
57  
58  
59  
60  
61  
62  
63  
64  
65

[35] E.E. de Obaldia, C. Jeong, L.K. Grunenfelder, D. Kisailus, P. Zavattieri, Analysis of the mechanical response of biomimetic materials with highly oriented microstructures through 3D printing, mechanical testing and modeling, *Journal of the Mechanical Behavior of Biomedical Materials* 48 (2015) 70-85.

[36] I. Petrov, P.B. Barna, L. Hultman, J.E. Greene, Microstructural evolution during film growth, *Journal of Vacuum Science & Technology A* 21(5) (2003) S117-S128.

[37] C.J. Li, A. Ohmori, Relationships between the microstructure and properties of thermally sprayed deposits, *Journal of Thermal Spray Technology* 11(3) (2002) 365-374.

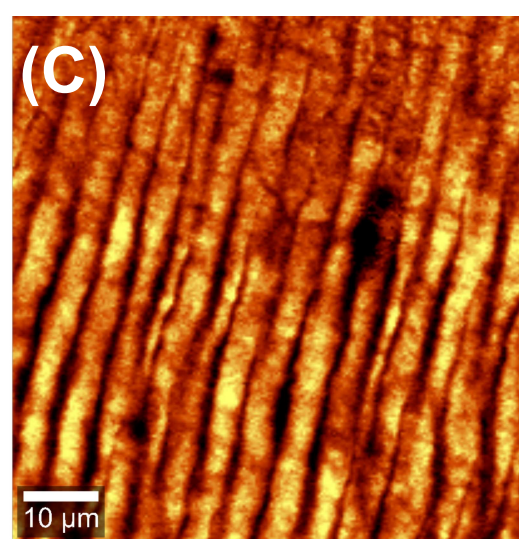
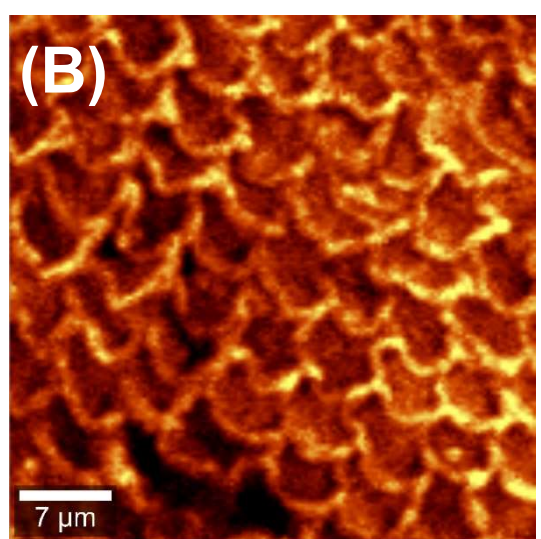
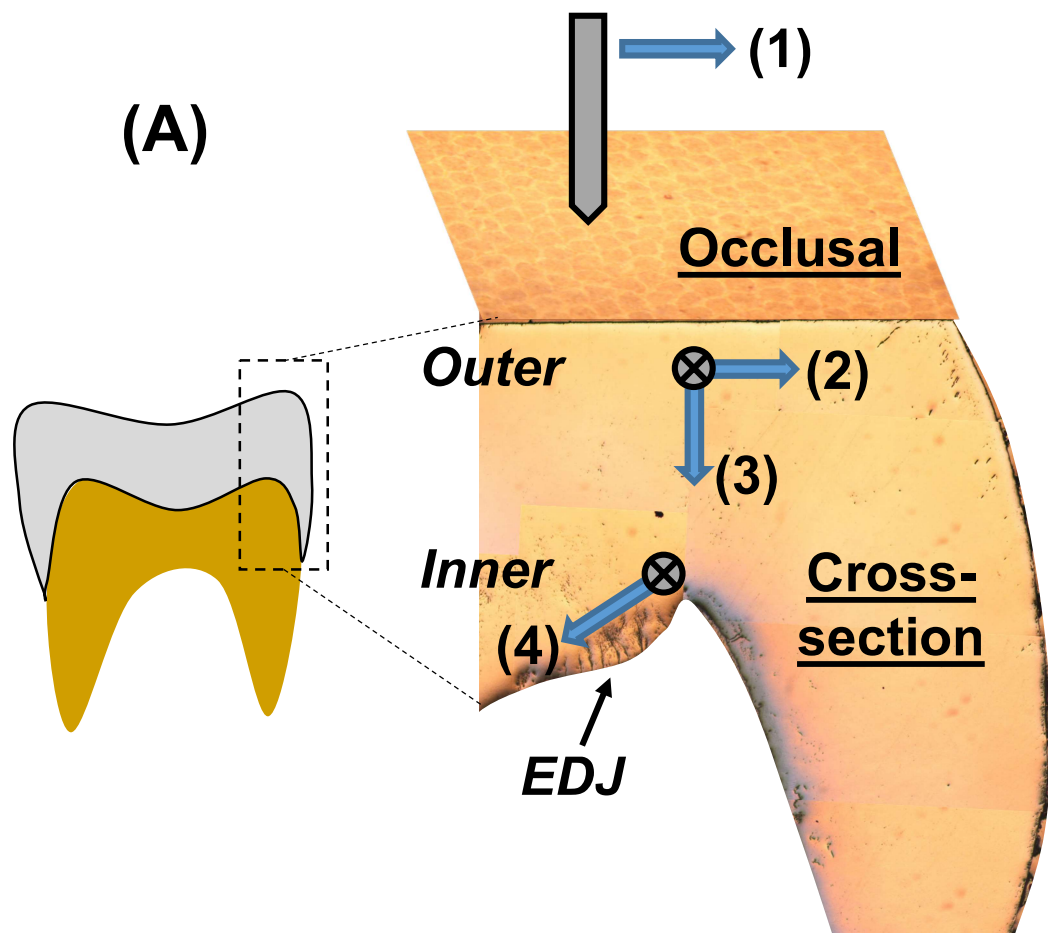


Figure 1

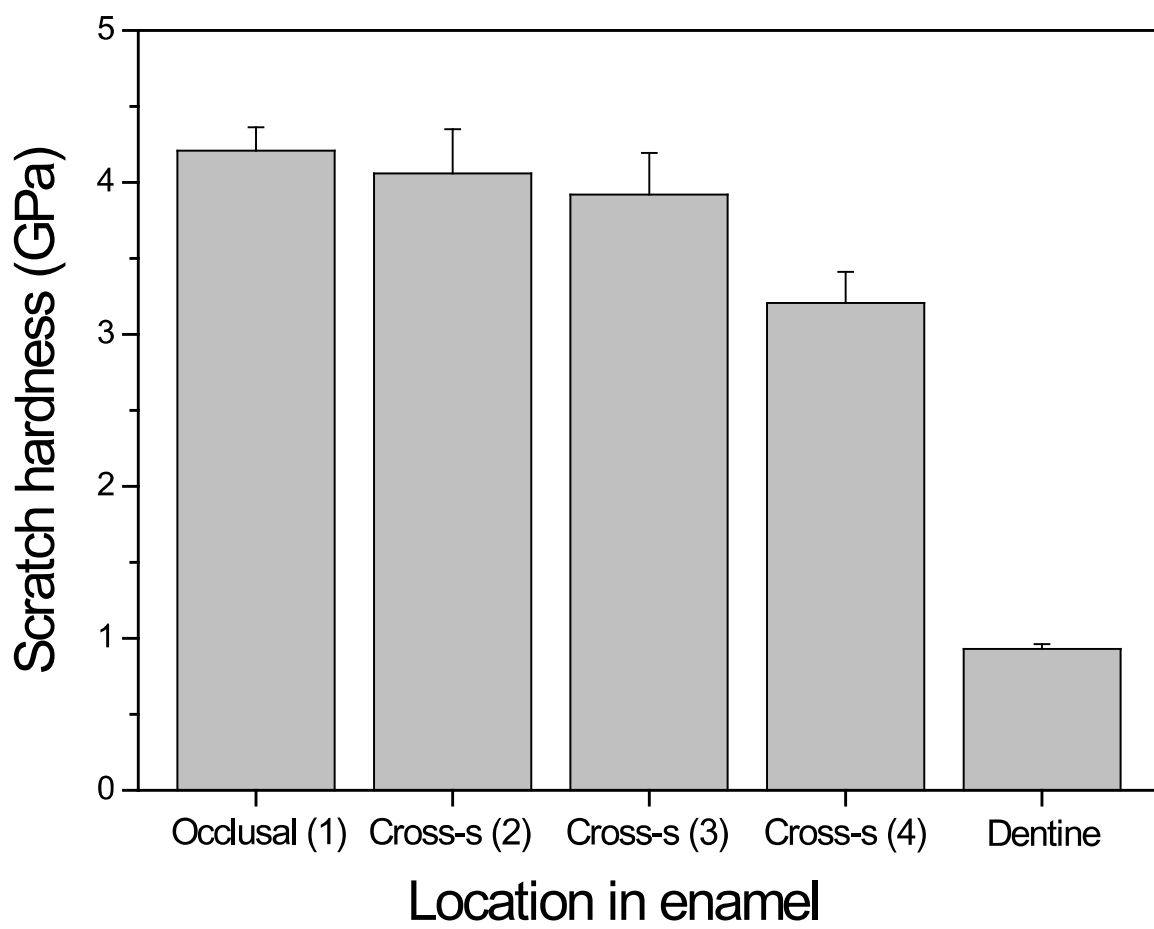


Figure 2

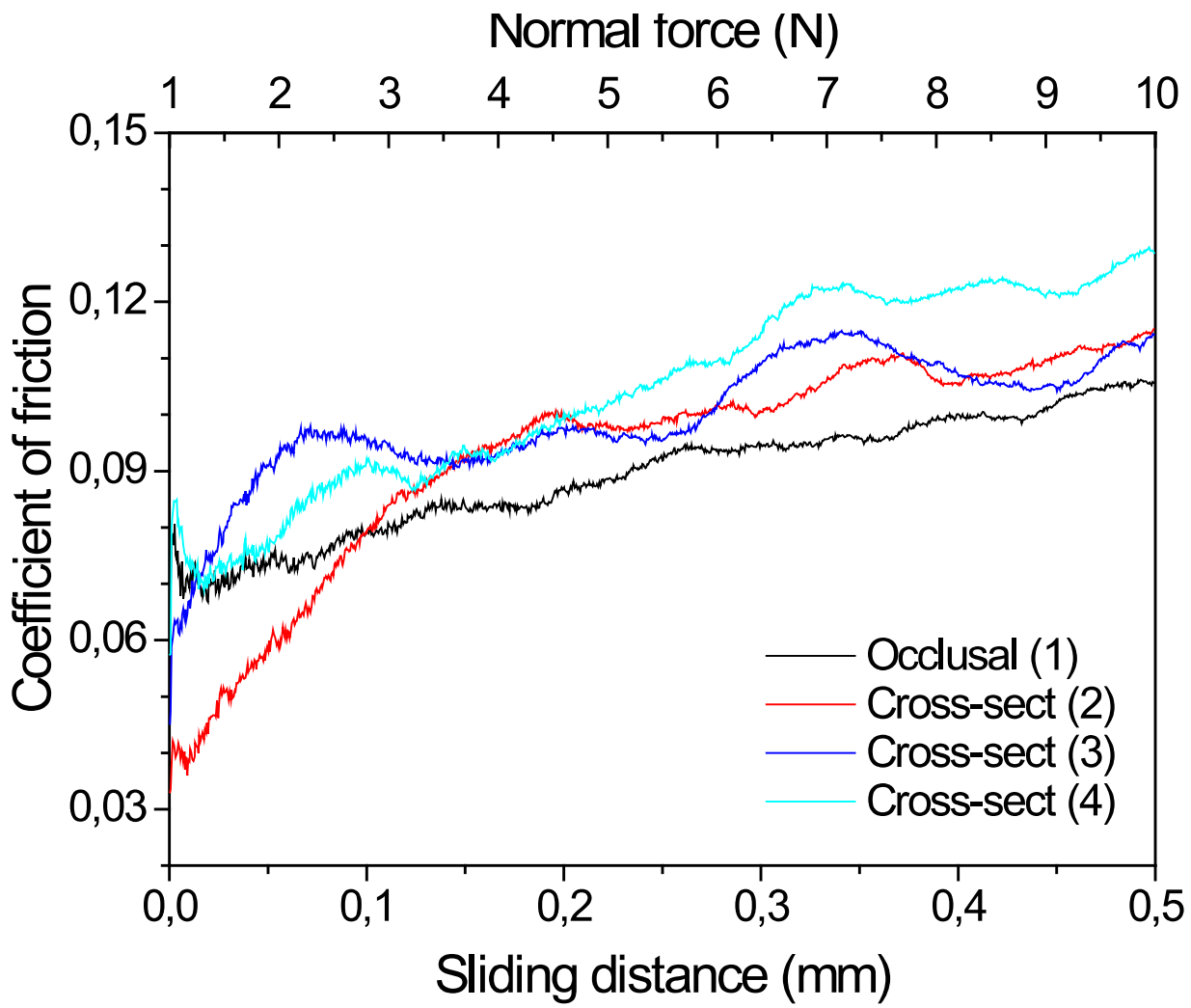


Figure 3

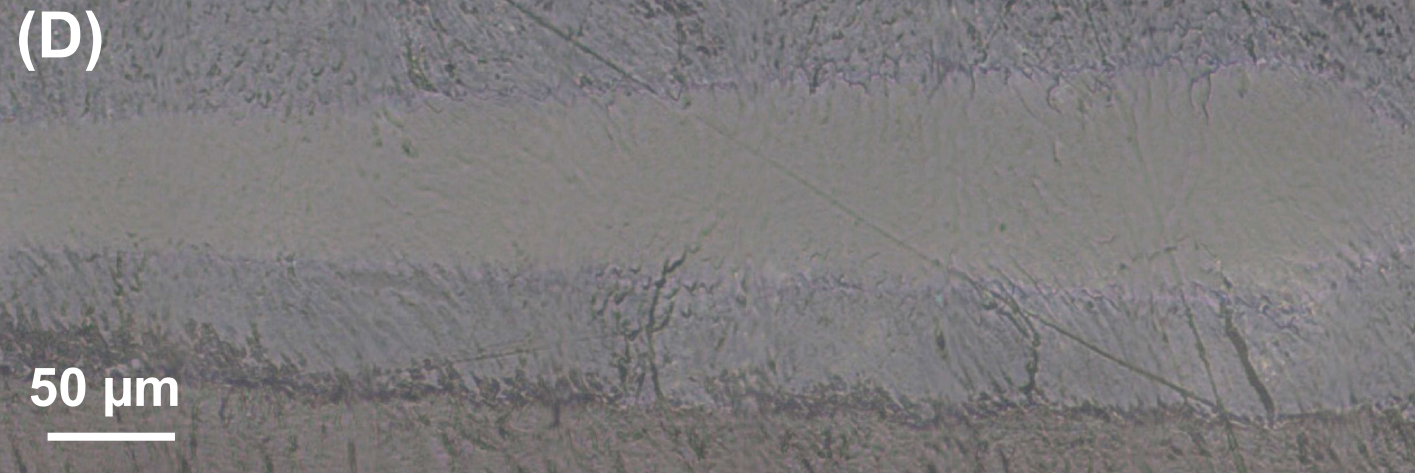
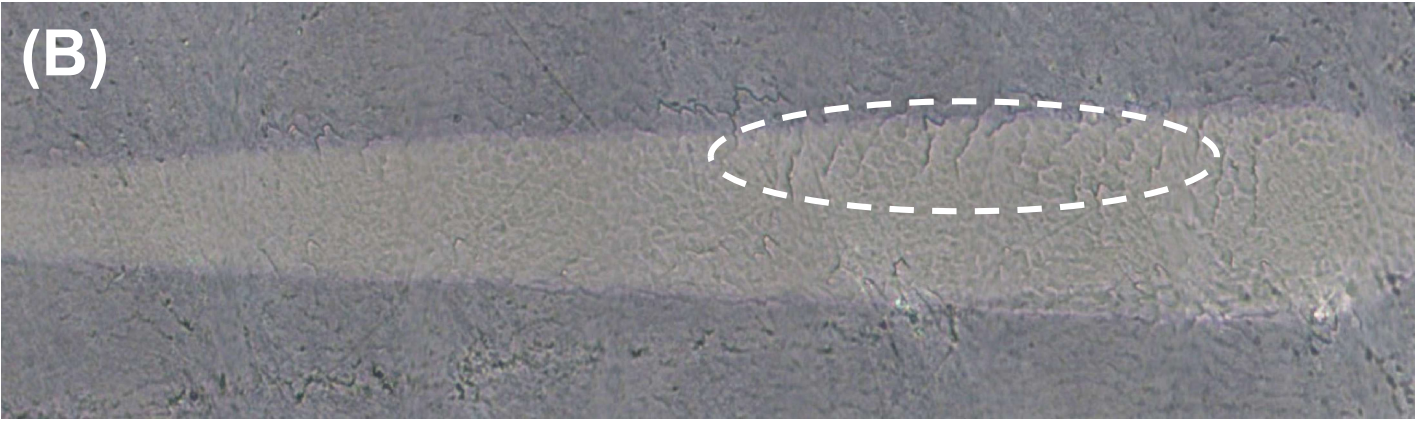
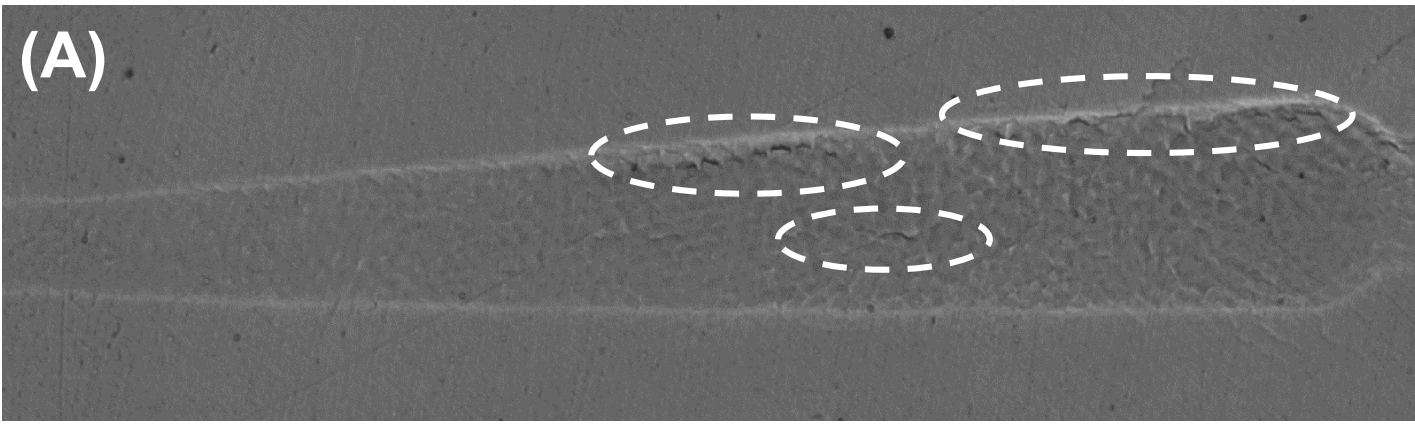


Figure 4



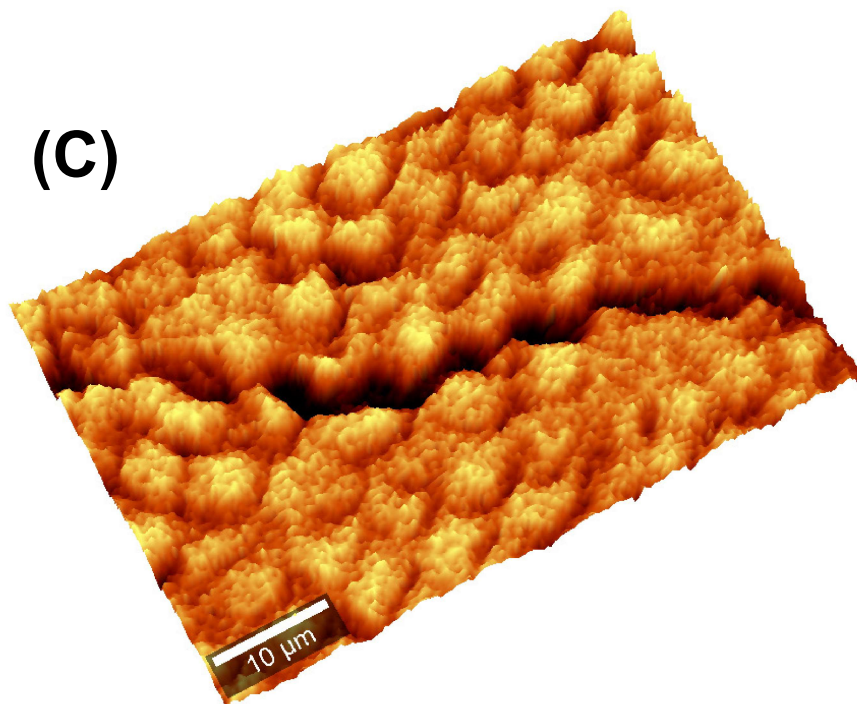
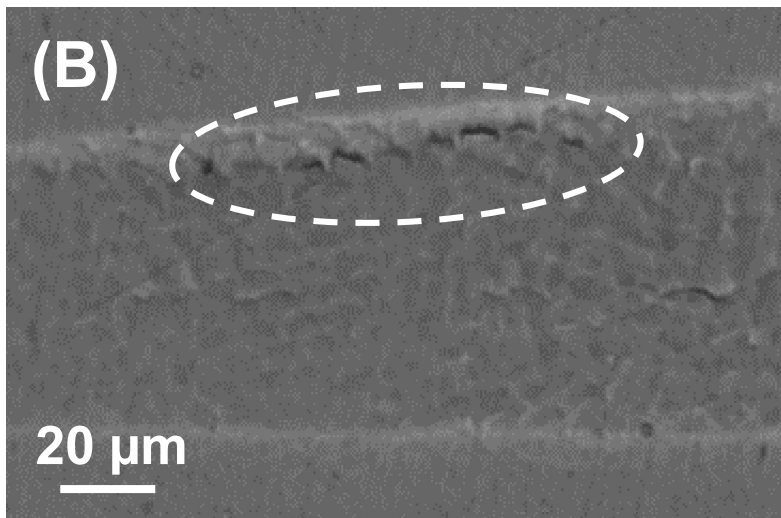
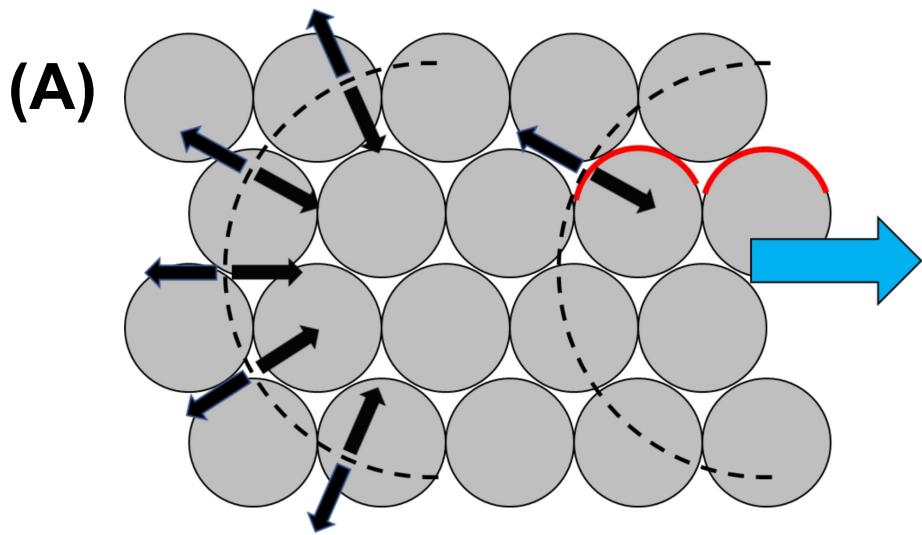


Figure 5

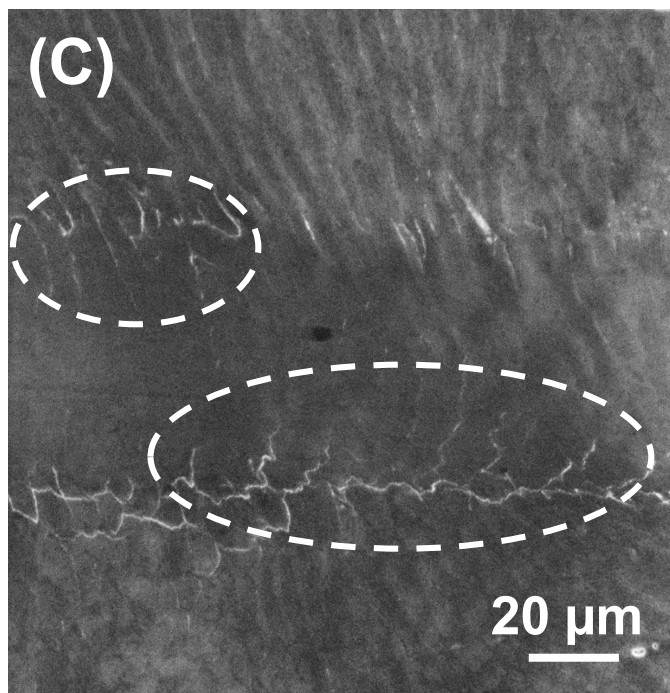
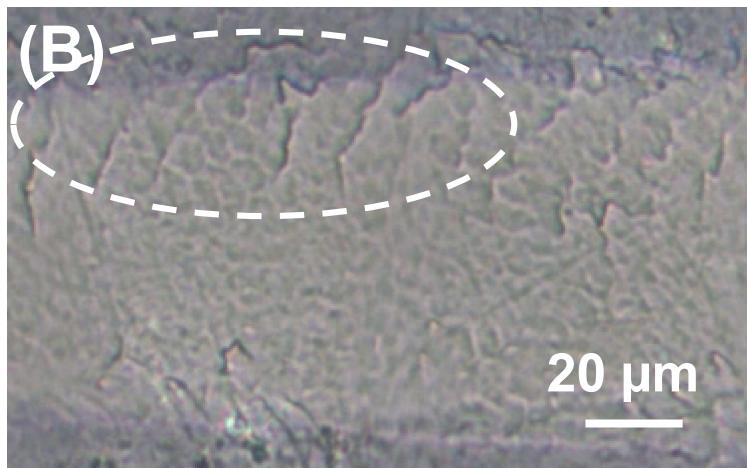
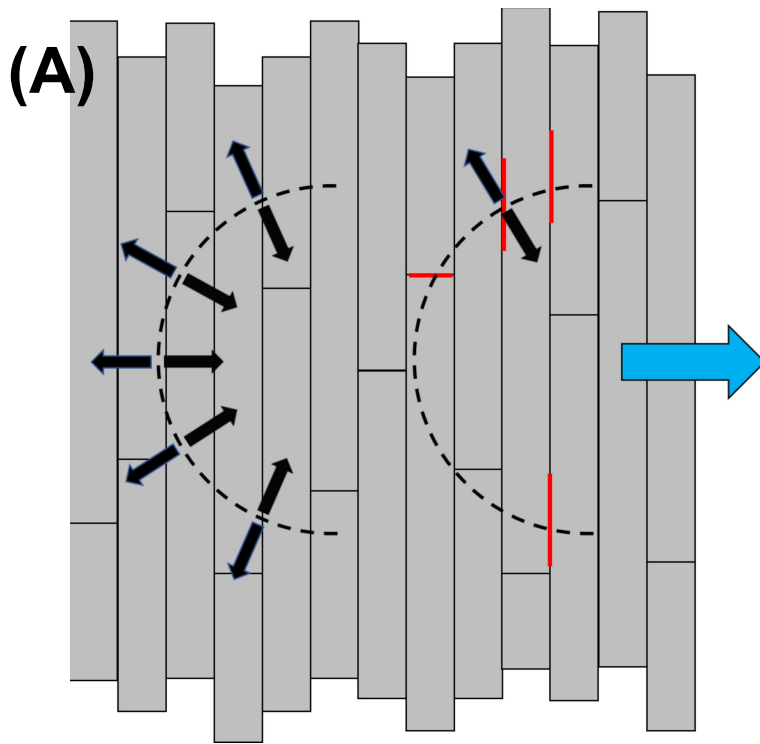


Figure 6

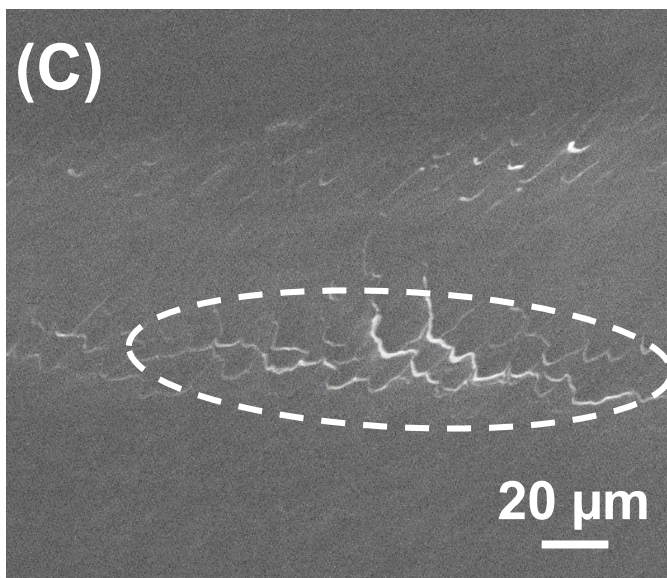
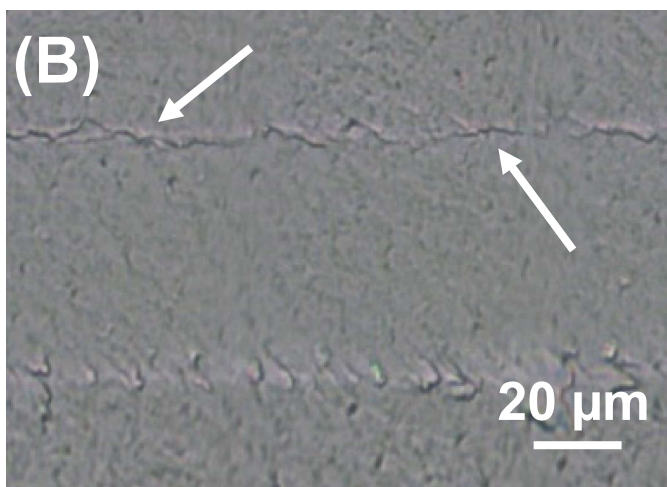
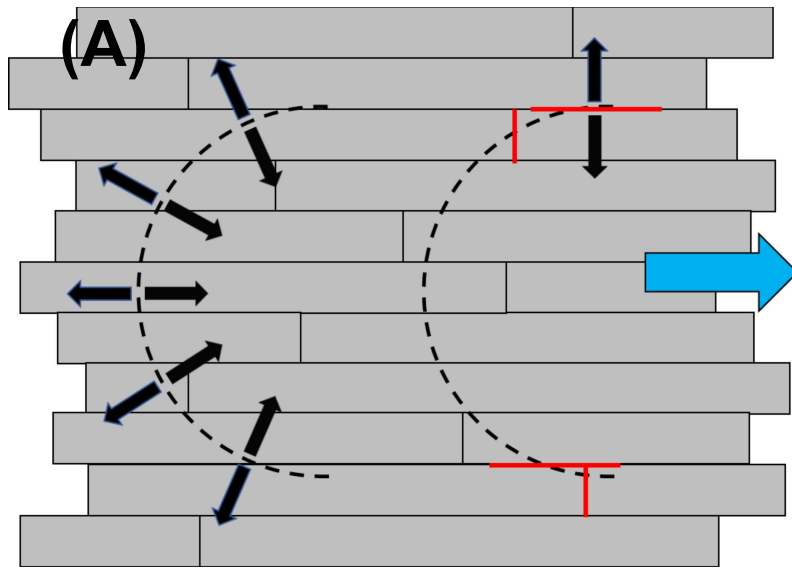


Figure 7